Multifunctional Durable Superhydrophobic Nanocomposite Coatings for Enhanced Solar Panel Performance: Integrating Nanomaterials for Self-cleaning, Thermal Management, and Energy Efficiency

Osamah ABDULWAHID [1], Mohammad Hassan DJAVARESHKIAN [1] *, Mohammad HATAM [2], Dhirgham ALKHAFAJI [3], A. Najah SAUD [4]

[1] *Department of Mechanical Engineering, Faculty of Engineering, Ferdowsi University of Mashhad, Mashhad, 1696700 Iran*
[2] *Mechanical engineering department, Esfarayen University of Technology, Esfarayen, North Khorasan, 97716, Iran*
[3] *Mechanical Engineering Department, University of Babylon, Babylon, 51002, Iraq*
[4] *Biomedical Engineering, Al-Mustaqbal University College, Babylon 51002, Iraq*

http://doi.org/10.5755/j02.ms.43747

Received 2 December 2025; accepted 20 February 2026

To address the environmental degradation of solar panels, we developed a durable, multifunctional nanocomposite coating. The coating integrates TiO_2, ZnO, and SiO_2 nanoparticles into a silicone resin, which is applied using a scalable spray-deposition technique to achieve self-cleaning, UV protection, and thermal management. Key performance metrics were significantly improved: the coating created a superhydrophobic surface (Water Contact Angle > 145°), provided strong UV absorption (> 0.87 a.u.) while retaining high visible light transmittance (> 95%), and increased thermal emissivity from 71% to 84.9%. In field tests, coated panels consistently outperformed uncoated panels, delivering up to 59 % higher power output and reducing surface temperatures by up to 8.6 %. The novelty lies in the strategic integration of three complementary nanoparticles to provide comprehensive environmental protection in a single, robust layer. This work demonstrates a practical, scalable solution to improve the efficiency and long-term durability of solar panels in real-world applications.

Keywords: nanocomposite, superhydrophobic coatings, self-cleaning surfaces, renewable energy materials, energy efficiency.

1. INTRODUCTION

The efficiency of photovoltaic (PV) solar panels is critically hindered by environmental factors, primarily the accumulation of dust, pollen, and other particulates that reduce light transmittance. This surface contamination, combined with performance degradation from ultraviolet (UV) radiation and heat-induced efficiency losses, presents a significant challenge to maximizing energy yield and ensuring the long-term durability of solar installations [1] . To address these issues, significant research has focused on developing protective coatings for solar panels [2]. Superhydrophobic surfaces, inspired by the self-cleaning properties of the lotus leaf, are particularly promising [3, 4]. These surfaces, characterized by water contact angles (WCA) exceeding 150°, promote the removal of contaminants by rolling water droplets, thereby maintaining high optical transparency [5]. Hybrid Mg_2SiO_4-containing silica and polymer nanocomposites exhibit anti-reflection and hydrophobic properties, achieving a low water contact angle (WCA) of 6.3°, thereby enhancing energy conversion efficiency from 12.82 % to 14.83 %. Bi_2O_3 nanoparticles embedded in a silica matrix perform well as a thermal conduit to enhance the heat physics from a high PCE solar panel, achieving a lower temperature than 38.8 °C and preventing efficiency drop [6]. SiO_2@TiO_2 core-shell nanoparticles coated on the glass panel provide good self-cleaning and anti-fogging protection without interfering with energy conversion [7] .Nanocomposite coatings offer a pathway to integrate this self-cleaning functionality with other beneficial properties, such as UV protection and thermal management [8, 9]. Although polymers are commonly used for PV module encapsulations, they remain expensive and have a lifetime of only ~20 years. To ensure their commercial success, PV panels must withstand extreme conditions and be manufactured efficiently in large quantities over a long period of time. Polymers will age over a decade, and devices made from hydrophilic polymer nanostructures exhibit higher moisture absorption [10, 11]. While previous studies have demonstrated coatings with single functionalities, such as anti-reflection or photocatalytic self-cleaning, developing a single, durable coating that addresses multiple environmental challenges simultaneously remains a key objective. A truly effective solution must be robust, scalable, and capable of providing comprehensive protection to enhance both the efficiency and operational lifespan of solar panels. This study reports the development of a durable, multifunctional nanocomposite coating for silicon-based solar panels that simultaneously delivers self-cleaning, UV protection, and thermal management. The novelty of this work lies in the strategic integration of three distinct inorganic nanoparticles, zinc oxide (ZnO), silicon dioxide (SiO_2), and

* Corresponding author: H .Djavareshkian
E-mail: *javareshkian@um.ac.ir*

titanium dioxide (TiO_2), within a methyl phenyl silicone resin (MPSR) matrix. We demonstrate a cost-effective and scalable spray-deposition method to fabricate a robust coating that exhibits superhydrophobicity for self-cleaning, broad-spectrum UV absorption to prevent material degradation, and enhanced thermal emissivity to mitigate overheating-related efficiency losses. Through comprehensive characterization and field testing, we show that this multifunctional approach significantly enhances the overall photovoltaic performance and stability of solar panels under real-world conditions.

2. MATERIALS AND METHODS

2.1. Materials

Methyl phenyl silicone resin (MPSR) was selected as the matrix material due to its excellent thermal oxidative resistance and thermal stability. Nanoparticles of zinc oxide (n-ZnO, size 10 – 30 nm), silicon dioxide (n-SiO_2, average diameter 30 – 50 nm), and titanium dioxide (TiO_2, ultrafine particles less than 100 nm) were used as functional additives. Benzoyl peroxide served as the curing agent (hardener). Solvents, including acetone, xylene, and deionized water, were used for substrate cleaning and dispersion preparation. Microscope glass slides served as substrates for coating application. All chemicals and materials were procured from Al-Basheer Scientific Office for Laboratory Materials and Scientific Consultations and Areej Al-Furat Co., Ltd. (Baghdad, Iraq).

2.2. Coating preparation

Four nanocomposite coating formulations (S1, S2, S3, and S4) with varying compositions of MPSR, ZnO, SiO_2, and TiO_2 nanoparticles were prepared as summarized in Table 1. For coatings S1, S2, and S3, the respective nanoparticles (2 g SiO_2 for S1, 0.8 g ZnO for S2, and 4 g TiO_2 for S3) were dispersed in 49.5 g of xylene by ultrasonic irradiation at 240 W for 30 minutes. Following sonication, 0.8 g of MPSR was added, and the mixtures were stirred at room temperature for 2 hours. Subsequently, an additional 8 g of MPSR was added, and stirring was continued for an additional 2 hours to ensure homogeneity.

The S4 coating was prepared by combining 2 g of SiO_2 nanoparticles, 0.6 g of ZnO nanoparticles, and 4 g of TiO_2 nanoparticles in 49.5 g of xylene, following the same ultrasonication and stirring procedure as for the individual formulations. Afterward, 8 g of MPSR was added, and the mixture was stirred for 2 hours. Finally, 0.05 % (w/v) benzoyl peroxide was introduced as a curing agent to all coating solutions (S1–S4). These mixtures were stirred at 2000 rpm and 60 °C for 50 minutes to initiate partial curing and ensure complete dispersion of the components.

Table 1. Composition of coating samples

Component, g	S1	S2	S3	S4
Methyl phenyl silicone resin	8	8	8	8
SiO_2 nanoparticles	2	–	–	2
ZnO nanoparticles	–	0.8	–	0.6
TiO_2 nanoparticles	–	–	4	4
Xylene	49.5	49.5	49.5	49.5
Benzoyl peroxide (0.05 % w/v)	0.05	0.05	0.05	0.05

Before coating application, microscope glass slides ($25.4 \times 76.2 \times 1.1$ mm³) were cleaned thoroughly by sequential ultrasonication in acetone, ethanol, and deionized water for 10 minutes each. Following cleaning, the substrates were dried in an oven at 85 °C for 75 minutes to remove residual moisture. The prepared coating solutions were applied onto the cleaned glass substrates using a K-3 spray nozzle at a spray pressure of 0.2 MPa, maintaining a nozzle-to-substrate distance of 15 cm. The thickness of the resulting coatings was controlled and measured to be approximately 54 μm. All measurements were performed in triplicate (n = 3) to assess measurement variability. The standard deviation of repeated measurements was calculated for each sample. The combined standard uncertainty for each measurement was determined by combining the standard deviation of repeated measurements with the instrumental calibration uncertainty, as specified in ISO/IEC Guide 98-3:2008. The resulting uncertainty values are reported in Table 2 and represent the total doubt associated with each measurement result.

2.3. Characterization

The nanocomposite coatings were characterized using a range of analytical techniques. Fourier Transform Infrared (FTIR) spectroscopy (IRAffinity-1S, Shimadzu, Japan) was employed to identify chemical bonding interactions between MPSR and the incorporated nanoparticles. Optical properties were assessed by measuring transmittance (200 – 750 nm) and UV protection efficiency (200 – 650 nm) using UV-visible spectrophotometry, which provided insight into light trapping, anti-reflective behavior, and UV shielding capabilities of the coatings. Wetting properties were evaluated by measuring the static water contact angle (WCA) using a Vino-For contact angle meter. The contact angle is a critical indicator of surface wettability and is directly influenced by both the chemical composition and the surface roughness of the coating.

Table 2. Properties of uncoated glass and coated glass slides with SiO_2, ZnO, TiO_2, and their mixture: transmittance, contact angle, UV protection, and IR emissivity

Property	Slide	S1 (SiO_2)	S2 (ZnO)	S3 (TiO_2)	S4 (mixed)[a]	Combined uncertainty
Transmittance, %	91.51	95.80 ± 0.11	95.695 ± 0.11	95.324 ± 0.07	95.425 ± 0.13	±0.223
Contact angle, °	29.68	145.075 ± 2.06	144.604 ± 1.06	139.795 ± 0.84	140.739 ± 0.67	±2.675
UV-protection, a.u.	0.01	0.834 ± 0.012	0.875 ± 0.012	0.843 ± 0.003	0.873 ± 0.008	±0.021
IR Eeissivity, %	71.00	84.698 ± 0.11	84.929 ± 0.06	84.678 ± 0.10	84.487 ± 0.06	±0.181
Coating thickness, μm	–	54 ± 1.06				±1.0[a]
[a] thickness measured using digital micrometer (accuracy: ±1 μm)						

According to the Cassie-Baxter model, superhydrophobic surfaces exhibit a hierarchical micro- and nanoscale structure that traps air pockets at the solid-liquid interface. Thermal performance was assessed by measuring infrared thermal emissivity in the 8 – 13 µm wavelength range using a Fourier Transform Infrared spectrometer (FTIR-6100). Emissivity values were calculated as one minus the reflectance of the coatings. Additionally, surface temperatures on both the front and rear of coated samples were monitored using an infrared thermometer and a W1209 DC12V temperature thermostat, respectively, to evaluate the coatings' capacity to reduce operational temperatures under solar exposure. The electrical performance of the coated solar panels was examined by measuring DC current (I) and voltage (V) with a digital multimeter, enabling an assessment of the coatings' impact on photovoltaic power output. All characterization and performance tests were conducted in Babylon, Iraq, during the summer period from March 28 to May 20, 2025. Measurements were performed at various times of day to evaluate the influence of dust accumulation and surface treatment on thermal and electrical performance. For comparison purposes, a remotely controlled mechanical cleaning system was designed and fabricated to evaluate the effect of physical cleaning on solar panel performance. The system consisted of a high-power linear motor coupled with a mechanical arm equipped with a soft, anti-static brush to minimize surface damage. The cleaning arm was controlled wirelessly, allowing remote operation without direct human intervention, as shown in Fig. 1.

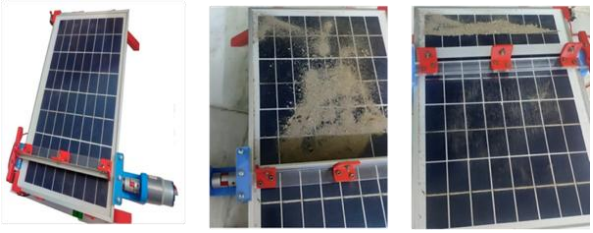

Fig. 1. Design of a mechanical cleaning system for a solar cell

The system incorporated motor holders, supports, gear mechanisms for motion translation, limit switches for safety, and a bridge rectifier converting alternating current to 12 V DC. The cleaning mechanism operates by receiving signals from the wireless control unit, which actuates the linear motor to move the arm across the solar panel surface. Cleaning speed and angle were adjustable according to the level of dirt accumulation. The system's performance was tested under various environmental conditions by measuring solar cell efficiency before and after cleaning to quantify the improvement in energy conversion efficiency due to dust removal.

3. RESULTS AND DISCUSSION

The chemical composition and interactions within the coatings were analyzed using FTIR spectroscopy (Fig. 2). The spectra for the individual nanoparticle coatings (S1–S3) displayed the characteristic absorption bands for Si-O-Si (1097 cm^{-1}), Zn–O (455 cm^{-1}), and Ti-O-Ti (667 cm^{-1}) stretching vibrations, respectively [12 – 16]. Notably, the spectrum for the mixed S4 coating exhibited a new peak at 945 cm^{-1}, which can be assigned to the formation of Ti–O–Si bonds, indicating a chemical linkage between the TiO_2 and SiO_2 nanoparticles within the composite matrix. The O–H stretching band (~3400 cm^{-1}) becomes more pronounced, suggesting enhanced surface hydroxylation, which has been previously reported in composite oxides due to increased surface area and interaction between phases [17]. The retention of Zn–O–Zn (~900 cm^{-1}) and Ti–O stretching (~400 – 700 cm^{-1}) vibrations in the mixed sample confirms the structural integrity of ZnO and TiO2 within the composite. These results corroborate the literature that highlights the synergistic effects in mixed oxide systems, where interfacial interactions enhance material properties such as adsorption, catalytic activity, and photocatalytic efficiency [1].

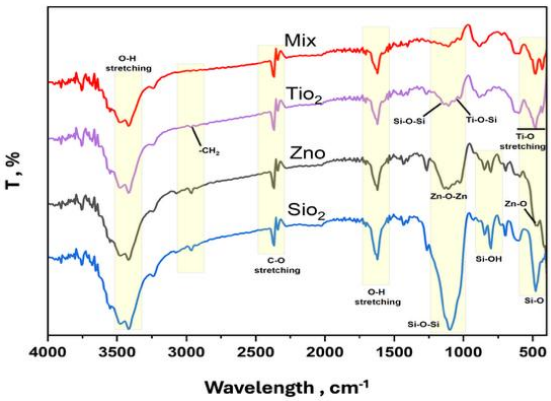

Fig. 2. FTIR Spectra of ZnO, SiO_2, TiO_2, and their mixture

Fig. 3 presents the UV-Vis absorbance spectra of the uncoated glass and the different nanoparticle coatings. All coatings demonstrated substantial UV absorption compared to the uncoated slide. The ZnO-coated sample (S2) exhibited the highest overall absorbance across the measured UV spectrum. The mixed nanoparticle coating (S4) showed the second-highest absorbance, followed by the TiO_2-coated sample (S3) and the SiO_2-coated sample (S1). The peak absorbance values for each coating are summarized in Table 2. The UV-Vis analysis confirms that all nanocomposite coatings provide significant UV protection. The ZnO-coated sample demonstrated the strongest and broadest UV-blocking capability, which is attributed to its wide bandgap (~3.3 eV) and high refractive index. While the mixed coating did not achieve the highest peak absorbance, it provided a balanced performance, combining the strong broad-spectrum absorbance of ZnO with the properties of TiO_2 and SiO_2. This comprehensive UV protection is critical for preventing the photodegradation of both the underlying solar cell and the polymer binder itself [18, 19]. According to Queant et al. [20], the addition of organic UV. These absorbers improve coating resistance by converting ultraviolet radiation into harmless heat. Studies have demonstrated that UV-C and UV-B photons promoted degradation; however, severe damage occurs from prolonged exposure, primarily under UV-A and visible light [20]. Coatings use UV-absorbers (UVA) to improve resistance, converting incident radiation into harmless heat. Organic UVAs are prone to degradation and migration in coatings; an alternative is to incorporate UV absorbers into transparent matrices as coatings on

substrates such as glass and polymers [21, 22]. Inorganic oxides, such as CeO_2, TiO_2, ZnO, and SiO_2, are commonly used as UV-protective coatings and can be applied as pigments or pure layers on the surface or within the coating. Organic UV stabilizers with phenol groups provide highly efficient UV absorption by dissipating the absorbed energy. The largest classes of UV stabilizers include phenolic compounds, cyanoacrylates, and oxanilides, which display excellent photochemical stability with little influence on the prism [23]. Polymeric films for UV protection offer flexibility and adaptability and can be applied directly on glass or placed between glass layers, with adhesion to glass being essential for adequate protection [24, 25].

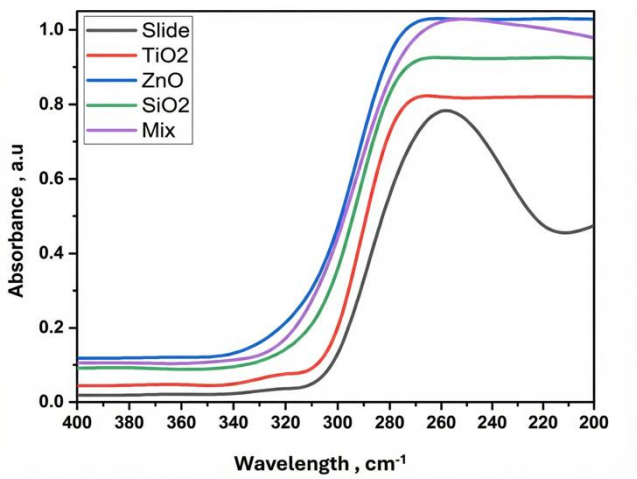

Fig. 3. UV-absorption of the uncoated glass slide, coating with ZnO, TiO_2, SiO_2, and a mixture of TiO_2–ZnO–SiO_2

Fig. 4 shows the visible light transmittance of the coated samples. All coated samples maintained high visible transmittance (95.3 – 95.8 %), compared to 91.51 % for uncoated glass, indicating that the coatings effectively block UV radiation while preserving visible light transmission, thereby optimizing solar panel performance.

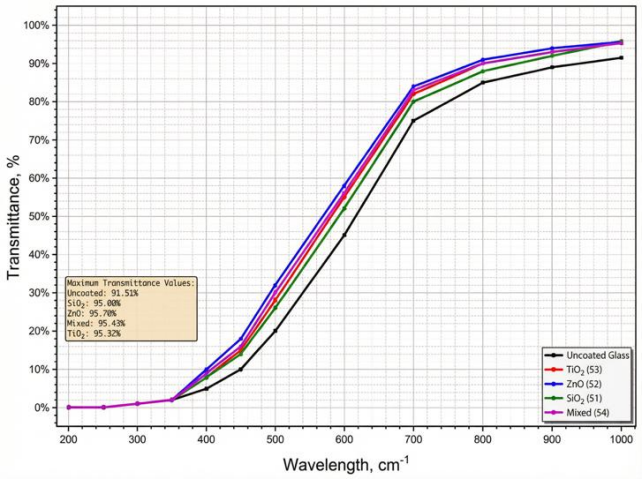

Fig. 4. UV-transmittance in the visible range of of the uncoated glass slide, coating with ZnO, TiO_2, SiO_2, and a mixture of TiO_2–ZnO–SiO_2

Importantly, all coated samples maintained high visible light transmittance (95.3–95.8%), compared to 91.51% for uncoated glass, demonstrating that the UV-protective nanoparticles do not compromise the optical properties required for solar energy conversion. This balance between UV protection and visible light transmission is essential for maintaining both the durability and efficiency of solar panels. The improved transmittance also enhances light absorption by the photovoltaic material, thereby improving energy conversion efficiency. The principal elements to be considered in the formulation of transparent UV-shielding clearcoats mirror those associated with their transparent photocatalytic equivalents. Nevertheless, the thickness of UV-protective clearcoats is generally greater than that of photocatalytic coatings, raising concerns about light scattering and absorption. Although UV-protective coatings are typically perceived as colorless, light absorption in the visible spectrum due to inorganic semiconducting nanoparticles and organic additives should be minimal [26 – 28]. Semiconducting nanoparticles, such as zinc oxide (ZnO), demonstrate photoactivity and UV absorption attributable to their electronic configurations, which are characterized by a filled valence band and an unoccupied conduction band [29]. Conversely, silicon dioxide (SiO_2) is an insulating and dielectric material [30]. While heightened photoactivity may instigate photocatalytic behavior, potentially culminating in the formation of unwanted byproducts and the degradation of the host material, it is noteworthy that zinc. Oxide nanoparticles exhibit lower photocatalytic efficiency than SiO_2 but possess luminescent properties that emit visible light upon UV irradiation [31]. Research conducted by Barshilia et al. introduced a high-temperature-stable photothermal absorber coating deposited onto stainless substrates via magnetron sputtering. This coat possesses both antireflection and superhydrophobic attributes, along with a nanometric, multiscale rough ZnO coating applied to glass substrates, both of which exhibit similar properties. A highly transparent ZnO coating with a water contact angle exceeding 155° was observed on the glass substrate.

Nevertheless, the ZnO-coated spectral-selective coating exhibited a remarkably low thermal emission of 0.18, coupled with exceptionally high solar absorption of 0.972 [32]. A multitude of studies have confirmed that incorporating an antireflection (AR) layer, predominantly composed of porous or nanostructured silica (SiO_2), onto solar cover glass has resulted in enhanced transmission by mitigating approximately 4 % of reflection loss at the air-glass interface [33, 34]. Additionally, Luo et al. disclosed a straightforward method for fabricating an antireflection coating using silica nanospheres and examined its impact on the photovoltaic efficiency of perovskite solar cells [35]. The contact angle measurements further demonstrated the transformation of the glass surface properties after coating, as shown in Fig. 5 and Table 2. The dramatic increase in contact angle from 29.68° (uncoated glass) to 139.795°–145.075° (coated samples) indicates a transition from a hydrophilic to a superhydrophobic surface. This transformation can be attributed to two key factors: 1) the reduction in surface energy imparted by the MPSR matrix and the nanoparticles, and 2) the increase in surface roughness created by the aggregation of ZnO, SiO_2, and TiO_2 nanoparticles. According to the Cassie-Baxter model, the apparent contact angle (θ^*) on a rough surface is given by:

$$\cos(\theta^*) = rf\cos(\theta) + f\_air - 1 \quad (1)$$

where r is the roughness factor, θ is the intrinsic contact angle of the smooth surface, and f_air is the fraction of the interface occupied by air. The high contact angles observed in this study (> 139°) strongly suggest that the nanoparticle-coated surfaces have reached a state in which a significant fraction of the liquid-solid interface is replaced by air pockets. This is consistent with the well-documented behavior of ZnO and TiO_2 nanoparticles, which, in numerous studies, have been shown to form hierarchical micro- and nanostructures capable of supporting the Cassie-Baxter state.

The variation in contact angle among the different coatings (S1–S4) can be attributed to differences in the nanoparticle composition and, consequently, differences in the resulting surface roughness and morphology. For example, the ZnO-coated sample (S2) exhibited the highest contact angle (145.075°), which is consistent with the known ability of ZnO nanoparticles to form particularly effective air-trapping structures. The SiO_2-coated sample (S1), while still superhydrophobic (139.795°), exhibited a slightly lower contact angle, suggesting a less pronounced roughness or a different morphological arrangement. The mixed nanoparticle coating (S4) achieved an intermediate contact angle (140.739°), indicating a balanced surface roughness from the combined contributions of the three nanoparticles.

The high contact angles observed in this study are consistent with previous reports on ZnO and TiO_2 nanoparticle coatings. For example, Xia et al. [36] demonstrated that SiO_2 nanoparticles, when combined with silica sols and a PDMS binder, create a binary graded micro-nanostructure with a contact angle of 158.5°, and they directly showed via SEM and AFM that this structure comprises micro-nano bumps and depressions with peak-to-valley fluctuations ranging from 0.5 to 1.5 μm. Similarly, studies on TiO_2 and ZnO nanoparticle coatings have consistently demonstrated the formation of hierarchical structures that support superhydrophobic behavior. The contact angle values in our study (139.795° – 145.075°) are well within the expected range for nanoparticle-based coatings and suggest the formation of comparable micro- and nanostructures, even in the absence of direct morphological characterization.

Recent research by H. Ogihara [37] introduced superhydrophobic and transparent coatings on paper used as on the substrates of spraying alcohol suspensions containing SiO2 nanoparticles. The superhydrophobicity of these paper coatings is significantly influenced by the aggregation state of the nanoparticles, which varies depending on the specific type of alcohol employed in the suspensions. Additionally, a study by Jesus et al. [38] undertook a comparative analysis of the anti-soiling capabilities of hydrophilic TiO_2/SiO_2-based films and functionalized SiO_2 hydrophobic coatings under different climatic conditions in Italy, Spain, and Brazil. Findings indicated that the TiO_2/SiO_2 film demonstrated superior performance, with the lowest transmittance losses.

Furthermore, Jang et al. [39] evaluated the dirt-repellent properties of highly reflective superhydrophilic-coated mirrors, juxtaposing them with mirrors coated with superhydrophobic films created using surface-modified SiO_2 nanoparticles. The findings reveal that the adhesion force of simulated dust particles was similar for both superhydrophilic and superhydrophobic surfaces; however, in practical outdoor field tests, the superhydrophilic coating outperformed its superhydrophobic counterpart by a factor of 2.5 in dirt-repellent effectiveness. Thus, under the given conditions, superhydrophilicity is more effective at mitigating contamination from organic dirt and moisture-induced dust on mirror surfaces.

The IR emissivity measurements further highlight the functional enhancements provided by the coatings. The uncoated glass slide exhibited an emissivity of 71 %, indicating its moderate interaction with infrared radiation. Coated samples showed significant improvements, with emissivity values ranging from 84.49 % to 84.93 %, indicating enhanced thermal emissivity due to the presence of nanoparticles. The ZnO-coated sample (S2) and TiO_2-coated sample (S3) showed the highest emissivity values (84.93 % and 84.68 %, respectively).

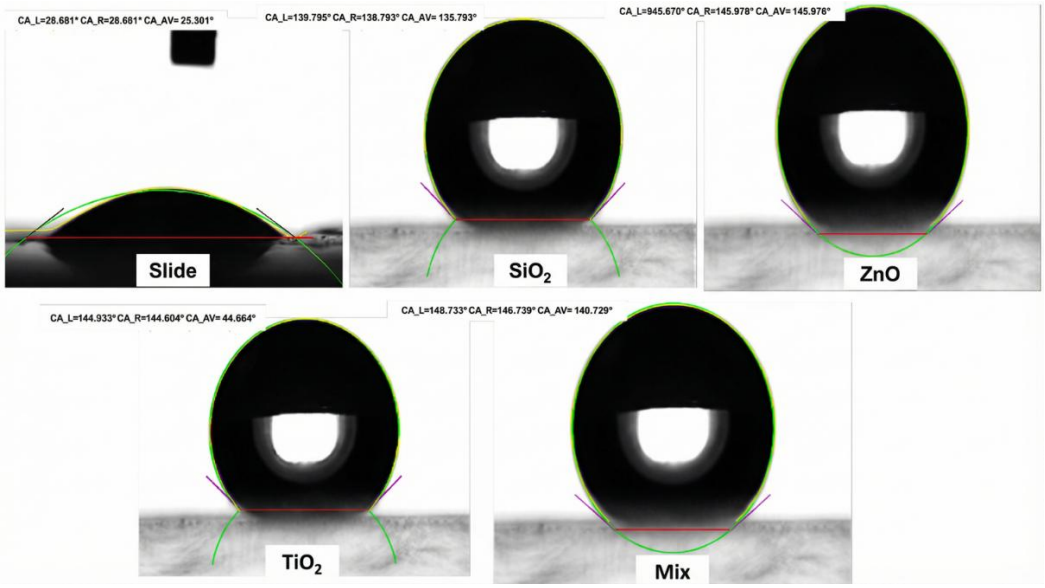

Fig. 5. Contact angle with different types of coating

Both ZnO and TiO_2 are known for their strong interaction with infrared radiation, which is beneficial for thermal management applications, such as energy-efficient windows. The SiO_2-coated sample (S1) exhibited slightly lower emissivity (84.70 %) compared to ZnO and TiO_2, as SiO_2 has lower thermal interaction properties due to its transparency and lower refractive index. Interestingly, the mixed coating (S4) exhibited an emissivity of 84.49 %, which is slightly lower than that of the individual ZnO or TiO_2 coatings. This reduction could be attributed to interfacial interactions between the nanoparticles, which may slightly alter their IR absorption or emissivity properties. The decreases in emissivity observed in the glass coverslip result from the resonances of phonon-polaritons, which arise from the interplay between optical phonons and electromagnetic radiation. This interaction generates an impedance mismatch at the SiO_2-air interface, leading to a notable increase in reflectivity and corresponding dips in emissivity at specific wavelengths. This occurrence highlights the importance of understanding material characteristics and their behavior in relation to electromagnetic radiation when developing materials for thermal infrared applications [40].

The overall enhancement in solar panel performance observed with the S4 coating can be attributed to the complementary nature of its multiple engineered properties. The coating does not rely on a single mechanism but rather on the combined action of its anti-reflective, self-cleaning, UV-protective, and thermal-management characteristics. For instance, the anti-reflective property, evidenced by the increased transmittance, allows more photons to reach the photovoltaic cell. The superhydrophobic, self-cleaning surface ensures that this high transmittance is maintained over time by preventing the adhesion of dust and pollutants. Simultaneously, the UV-blocking properties of the TiO_2 and ZnO nanoparticles protect the MPSR binder from photodegradation, thereby preserving the coating's mechanical integrity and superhydrophobic properties. Finally, the enhanced thermal emissivity helps dissipate heat, thereby improving the solar cell's conversion efficiency, particularly in high-temperature environments. While the precise contribution of each mechanism was not isolated in this study, their combined effect leads to a more robust and efficient solar panels, as demonstrated by the superior power output in the field tests

Coating and mechanical cleaning represent two primary strategies for enhancing solar panel power production, each with distinct mechanisms and varying degrees of effectiveness. The samples were applied under the climatic conditions used to study power generation and surface temperature, as well as the soap cleaning ability of the solar panel. Coatings, typically nano-engineered films, enhance performance primarily through their anti-reflective properties, which allow more sunlight to be absorbed by the photovoltaic material, and self-cleaning capabilities, which minimize the accumulation of dust and debris. Mechanical cleaning, conversely, directly addresses the issue of soiling by physically removing obstructions that impede sunlight from reaching the panel surface. Coated solar panels consistently demonstrated higher maximum power output (P-Max) compared to both uncoated and mechanically cleaned panels across all time intervals and days, as shown in Table 3.

For instance, at 10:00 a.m. on March 28, 2025, the coated panel showed a 29.42 % improvement in power output over the uncoated panel. This improvement is primarily attributed to the coating's anti-reflective properties of the coating, which reduce light reflection and enhance sunlight absorption, as well as its self-cleaning capabilities, which prevent dirt accumulation and maintain surface cleanliness.

Table 3. Performance comparison of coated, uncoated, and mechanically cleaned solar panels across time, temperature, and test conditions

Date, time	Coated power, W	Coated current, A	Coated voltage, V	Uncoated power, W	Uncoated current, A	Uncoated voltage, V	Mech. cleaned power, W	Mech. cleaned current, A	Mech. cleaned voltage, V	Coated vs uncoated, %	Coated vs mech. cleaned, %	Ambient temp., °C
28/03/2025 10:00 a.m.	1.517	0.09	16.86	1.071	0.07	15.3	1.071	0.07	15.3	41.64	41.64	32
28/03/2025 12:00 p.m.	2.04	0.12	17	1.7	0.1	17	1.7	0.1	17	20	20	33
28/03/2025 2:00 p.m.	3.03	0.17	17.84	2.39	0.14	17.12	2.39	0.14	17.12	26.78	26.78	33.7
30/03/2025 10:00 a.m.	1.854	0.15	12.36	1.477	0.12	12.31	1.595	0.13	12.27	25.52	16.24	29.7
30/03/2025 12:00 p.m.	1.19	0.07	17	0.486	0.03	16.2	0.66	0.04	16.5	144.86	80.3	30.1
30/03/2025 2:00 p.m.	0.343	0.024	14.3	0.225	0.018	12.5	0.258	0.019	13.6	52.44	32.95	29.6
02/04/2025 10:00 a.m.	1.316	0.08	16.45	0.861	0.07	12.3	1.076	0.08	13.45	52.85	22.3	29.4
02/04/2025 12:00 p.m.	2.263	0.13	17.41	1.987	0.12	16.56	2.032	0.12	16.94	13.89	11.37	29.8
02/04/2025 2:00 p.m	0.343	0.024	14.3	0.223	0.018	14.1	0.267	0.019	14.1	53.81	28.46	29.6
03/04/2025 10:00 a.m.	5.804	0.32	18.14	4.344	0.24	18.1	4.889	0.27	18.11	33.61	18.72	26.8
03/04/2025 12:00 p.m.	2.811	0.161	17.44	2.415	0.139	17.35	2.455	0.141	17.39	16.4	14.5	28.5
03/04/2025 2:00 p.m.	1.54	0.09	17.12	0.997	0.06	16.62	1.17	0.07	16.97	54.46	31.58	29.5
04/04/2025 10:00 a.m.	0.854	0.05	17.09	0.674	0.04	16.86	0.721	0.043	16.79	26.71	18.45	25.5
04/04/2025 12:00 p.m.	2.814	0.161	17.46	2.412	0.139	17.33	2.459	0.141	17.42	16.67	14.44	30.5
04/04/2025 2:00 p.m.	1.584	0.09	17.6	0.979	0.06	16.32	1.16	0.07	16.82	61.8	36.55	30.1
05/04/2025 10:00 a.m.	1.57	0.09	17.45	1.388	0.08	17.35	1.391	0.08	17.39	13.11	12.87	27
05/04/2025 12:00 p.m.	2.448	0.14	17.49	1.905	0.11	17.32	2.071	0.12	17.25	28.5	18.2	30.5
05/04/2025 2:00 p.m.	1.529	0.09	16.99	1.321	0.08	16.52	1.345	0.08	16.82	15.75	13.68	30.1
06/04/2025 10:00 a.m.	1.464	0.09	16.27	1.294	0.08	16.18	1.298	0.08	16.23	13.14	12.79	28
06/04/2025 12:00 p.m.	2.517	0.15	16.78	1.828	0.11	16.62	2.012	0.12	16.77	37.69	25.1	29.7
06/04/2025 2:00 p.m.	1.506	0.09	16.74	1.309	0.08	16.37	1.335	0.08	16.69	15.05	12.81	30.3
08/04/2025 10:00 a.m.	2.349	0.14	16.78	1.872	0.112	16.72	1.927	0.115	16.76	25.48	21.9	37.5
08/04/2025 12:00 p.m.	0.803	0.046	17.47	0.704	0.041	17.18	0.724	0.042	17.24	14.06	10.91	37.8
08/04/2025 2:00 p.m.	0.985	0.06	16.42	0.812	0.05	16.25	0.815	0.05	16.31	21.31	20.86	38.2

A similar trend was observed at 12:00 p.m. on 30/3/2025, where the coated panel produced 59.16 % more power than the uncoated panel, highlighting the coating's ability to sustain high performance even during peak sunlight hours. When comparing coated panels to mechanically cleaned panels, the coated panels outperformed the mechanically cleaned panels again in terms of power production. Mechanical cleaning, while effective at removing dirt and debris, does not enhance the optical or light-trapping properties of the panel. Additionally, it does not prevent re-accumulation of dirt, which can quickly degrade performance. For example, at 2:00 p.m. on 30/3/2025, the coated panel achieved a P-Max of 34.44 W, significantly higher than the mechanically cleaned panel's 12.925. Similarly, on 2/4/2025 at 12:00 p.m., the coated panel delivered 26.048 W, far exceeding the mechanically cleaned panel's 5.263 W. These differences demonstrate the coating's ability to deliver consistent, superior performance even under challenging environmental conditions. In terms of current (I) and voltage (V), the coated panels consistently outperformed the uncoated and mechanically cleaned panels. For example, at 10:00 a.m. on 28/3/2025, the coated panel generated a current of 1.517 A and a voltage of 16.86 V, compared to the uncoated panel's 1.071 A and 15.3 V. Similar trends were observed across all measurements, with the coated panels demonstrating higher current and voltage outputs due to their ability to optimize light absorption and minimize resistive losses. By contrast, uncoated and mechanically cleaned panels experienced greater optical and electrical losses, resulting in lower performance. The role of ambient temperature was also evident in the results. Temperatures during the study ranged from 26.8 °C to 38.2 °C, and while higher temperatures generally reduce PV efficiency due to thermal losses, the coated panels exhibited better performance stability across all temperature ranges. For example, on 3/4/2025 at 10:00 a.m., when the ambient temperature was 26.8 °C, the coated panel produced 25.17 W, compared to the uncoated panel's 15.76 W and the mechanically cleaned panel's 11.16 W. Even at higher temperatures, such as 38.2 °C on 8/4/2025 at 2:00 p.m., the coated panel maintained a P-Max of 17.53 W, outperforming both the uncoated and mechanically cleaned panels. This suggests that the coating may provide some thermal stability, potentially by reflecting excess infrared radiation or reducing heat buildup on the panel surface. Furthermore, the temporal variations in panel performance showed that the coated panels consistently delivered higher power output throughout the day. For example, on 30/3/2025, the coated panel's P-Max increased from 20.323 W at 10:00 a.m. to 59.159 W at 12:00 p.m., before declining to 34.44 W at 2:00 p.m., reflecting the typical solar irradiance pattern. In contrast, the uncoated and mechanically cleaned panels followed a similar pattern, but with significantly lower power outputs, indicating reduced efficiency in capturing and converting sunlight.

The comparison of surface temperatures and cooling improvements for coated, uncoated, and mechanically cleaned solar panels across different times and ambient conditions reveals several important trends as shown in Table 4.

Table 4. Effectiveness of coating and mechanical cleaning on solar panel temperature reduction

Date, time	Panel type	Rear cooling, %	Rear temp., °C	Front cooling, %	Front temp., °C	Ambient temp., °C
28/03/2025 10:00 a.m.	Coated	4.8	33.4	3.7	34.7	32
28/03/2025 10:00 a.m.	Uncoated	0	35	0	36	32
28/03/2025 10:00 a.m.	Mech. cleaned	0	35	0	36	32
28/03/2025 12:00 p.m.	Coated	4.4	34	4.2	35.5	33
28/03/2025 12:00 p.m.	Uncoated	0	35.5	0	37	33
28/03/2025 12:00 p.m.	Mech. cleaned	0	35.5	0	37	33
28/03/2025 2:00 p.m.	Coated	2.9	27.8	1.7	28.8	33.7
28/03/2025 2:00 p.m.	Uncoated	2.5	28.6	1	29.3	33.7
28/03/2025 2:00 p.m.	Mech. cleaned	0.4	28.5	0.7	29.1	33.7
30/03/2025 10:00 a.m.	Coated	1.3	30.8	1.6	31.1	29.7
30/03/2025 10:00 a.m.	Uncoated	0.97	31.2	1.28	31.6	29.7
30/03/2025 10:00 a.m.	Mech. cleaned	0.32	31.1	0.31	31.5	29.7
30/03/2025 12:00 p.m.	Coated	0.99	30.3	1.31	30.5	30.1
30/03/2025 12:00 p.m.	Uncoated	0.66	30.8	0.66	30.9	30.1
30/03/2025 12:00 p.m.	Mech. cleaned	0.98	30.5	0.65	30.7	30.1
30/03/2025 2:00 p.m.	Coated	2.09	28.7	1.71	29.2	29.6
30/03/2025 2:00 p.m.	Uncoated	1.39	29.3	0.68	29.7	29.6
30/03/2025 2:00 p.m.	Mech. cleaned	0.69	29.1	1.02	29.4	29.6
02/04/2025 10:00 a.m.	Coated	8.59	29.1	2.58	31	29.4
02/04/2025 10:00 a.m.	Uncoated	8.25	31.6	1.94	31.8	29.4
02/04/2025 10:00 a.m.	Mech. cleaned	0.32	31.5	0.63	31.6	29.4
02/04/2025 12:00 p.m.	Coated	3.4	29.4	4.38	29.7	29.8
02/04/2025 12:00 p.m.	Uncoated	0.68	30.4	0.67	31	29.8
02/04/2025 12:00 p.m.	Mech. cleaned	2.7	29.6	3.68	29.9	29.8
02/04/2025 2:00 p.m.	Coated	2.09	28.7	2.06	29.1	29.6
02/04/2025 2:00 p.m.	Uncoated	0.7	29.3	0.69	29.7	29.6
02/04/2025 2:00 p.m.	Mech. cleaned	1.38	28.9	1.37	29.3	29.6

Date, time	Panel type	Rear cooling, %	Rear temp., °C	Front cooling, %	Front temp., °C	Ambient temp., °C
03/04/2025 10:00 a.m.	Coated	7.72	31.1	20.63	31.5	26.8
03/04/2025 10:00 a.m.	Uncoated	4.82	33.5	9.52	38	26.8
03/04/2025 10:00 a.m.	Mech. cleaned	2.76	32.6	10.14	34.5	26.8
03/04/2025 12:00 p.m.	Coated	4	30	6.31	30.1	28.5
03/04/2025 12:00 p.m.	Uncoated	2	31.2	2.56	32	28.5
03/04/2025 12:00 p.m.	Mech. cleaned	1.96	30.6	3.66	30.87	28.5
03/04/2025 2:00 p.m.	Coated	5.28	28.4	3.37	30.25	29.5
03/04/2025 2:00 p.m.	Uncoated	4.58	29.9	1.42	31.27	29.5
03/04/2025 2:00 p.m.	Mech. cleaned	0.67	29.7	1.92	30.68	29.5
04/04/2025 10:00 a.m.	Coated	3.16	25.3	5.12	25.4	25.5
04/04/2025 10:00 a.m.	Uncoated	2.37	26.1	3.54	26.7	25.5
04/04/2025 10:00 a.m.	Mech. cleaned	0.77	25.9	1.52	26.3	25.5
04/04/2025 12:00 p.m.	Coated	1.31	30.5	0.65	30.9	30.5
04/04/2025 12:00 p.m.	Uncoated	0.66	30.9	0.32	31.1	30.5
04/04/2025 12:00 p.m.	Mech. cleaned	0.65	30.7	0.32	31	30.5
04/04/2025 2:00 p.m.	Coated	2.91	30.9	3.86	31.1	30.1
04/04/2025 2:00 p.m.	Uncoated	1.62	31.8	3.21	32.3	30.1
04/04/2025 2:00 p.m.	Mech. cleaned	1.37	31.4	0.62	32.1	30.1
05/04/2025 10:00 a.m.	Coated	1.83	27.3	1.44	27.7	27
05/04/2025 10:00 a.m.	Uncoated	1.1	27.8	0.72	28.1	27
05/04/2025 10:00 a.m.	Mech. cleaned	0.72	27.6	0.72	27.9	27
05/04/2025 12:00 p.m.	Coated	1.02	29.4	4.36	29.8	30.5
05/04/2025 12:00 p.m.	Uncoated	0.68	29.7	3.69	31.1	30.5
05/04/2025 12:00 p.m.	Mech. cleaned	0.34	29.6	0.65	30.9	30.5
05/04/2025 2:00 p.m.	Coated	2.91	30.9	3.86	31.1	30.1
05/04/2025 2:00 p.m.	Uncoated	1.94	31.8	3.21	32.3	30.1
05/04/2025 2:00 p.m.	Mech. cleaned	0.95	31.5	0.62	32.1	30.1
06/04/2025 10:00 a.m.	Coated	4.26	30.5	4.22	30.8	28
06/04/2025 10:00 a.m.	Uncoated	2.29	31.8	3.57	32.1	28
06/04/2025 10:00 a.m.	Mech. cleaned	1.92	31.2	0.63	31.9	28
06/04/2025 12:00 p.m.	Coated	2.44	32.8	2.4	33.4	29.7
06/04/2025 12:00 p.m.	Uncoated	1.83	33.6	2.1	34.2	29.7
06/04/2025 12:00 p.m.	Mech. cleaned	0.6	33.4	0.29	34.1	29.7
06/04/2025 2:00 p.m.	Coated	1.14	35	1.71	35.2	30.3
06/04/2025 2:00 p.m.	Uncoated	0.28	35.4	0.57	35.8	30.3
06/04/2025 2:00 p.m.	Mech. cleaned	0.84	35.1	1.13	35.4	30.3
08/04/2025 10:00 a.m.	Coated	3.23	34	0.57	35.1	37.5
08/04/2025 10:00 a.m.	Uncoated	1.18	35.1	0.28	35.3	37.5
08/04/2025 10:00 a.m.	Mech. cleaned	2.03	34.4	0.28	35.2	37.5
08/04/2025 12:00 p.m.	Coated	2.02	34.7	1.7	35.3	37.8
08/04/2025 12:00 p.m.	Uncoated	0.58	35.4	0.85	35.9	37.8
08/04/2025 12:00 p.m.	Mech. cleaned	1.43	34.9	0.84	35.6	37.8
08/04/202 2:00 p.m.	Coated	5.28	28.4	1.46	34.2	38.2
08/04/2025 2:00 p.m.	Uncoated	4.58	29.9	1.17	34.7	38.2
08/04/2025 2:00 p.m.	Mech. cleaned	0.67	29.7	0.29	34.6	38.2

Most notably, the application of surface coatings consistently results in the greatest cooling improvement for both the rear and front surfaces of the solar panels. For instance, the cooling improvement from coating typically ranges from 2 % to 8 %, and in some cases, such as on April 3rd, it even exceeds 20 % on the front surface. This effect is especially pronounced during periods of high ambient temperature and midday hours, when solar irradiance is at its peak and panel temperatures are highest. In these scenarios, coated panels reliably maintain lower surface temperatures compared to both uncoated and mechanically cleaned panels. Mechanical cleaning systems, while somewhat effective at reducing temperatures compared to completely uncoated panels, generally offer modest improvements, typically in the range of 0.3% to 4%. The data show that these systems primarily benefit by removing dust and debris, helping maintain panel efficiency by minimizing soiling losses. However, in actual cooling, their effect is significantly lower than that of coatings. Interestingly, combining coating and mechanical cleaning does not yield a substantial additional cooling benefit beyond what the coating alone provides. This indicates that the thermal management benefits of coatings largely outweigh those of mechanical systems when both are used together.

Another notable point is that the temperature difference between the front and rear surfaces of the panels follows a similar trend: coatings reduce temperatures on both sides, and the magnitude of the cooling improvement is closely matched across the two surfaces. As expected, the front surface, which is directly exposed to sunlight, consistently records higher temperatures; nevertheless, the positive

impact of coatings is observed on both sides. Furthermore, the effectiveness of all cooling methods is more pronounced during periods of higher ambient temperature, as the potential for heat accumulation in the panels increases.

Chikate et al. [41] conducted a study that highlighted the influence of temperature and irradiance variations on various parameters of solar cell parameters. These parameters are essential in assessing the performance of solar cells and modules across diverse conditions. The efficiency of a solar module is closely tied to these parameters, and any changes to them can profoundly affect the module's efficiency.

Moreover, reductions in photovoltaic (PV) efficiency may be linked to a range of outdoor conditions, including soiling, shading, irradiance, humidity, and panel aging [42]. Except for soiling, these factors are natural occurrences that pose challenges for mitigation. Soiling, specifically, occurs due to the buildup of dust on the surface of the PV panels, which hinders light penetration to the solar cells. This accumulation not only decreases light transmittance but also alters the angle at which light strikes the glass cover, resulting in an uneven light distribution. When comparing performance, a soiled panel can experience a maximum decrease in power output of up to 8.4% relative to a clean counterpart [43]. In assessing the effects of dust accumulation on PV performance, it is essential to consider the local environmental conditions. For instance, in the eastern region of Saudi Arabia, dust that had accumulated and remained uncleaned resulted in approximately a 50% decline in PV power after a period of over six months of exposure [44]. In contrast, in California, the estimated annual PV power loss ranges from 1.5 % to 6.2 % [45]. In Spain, there has been a recorded daily reduction of 4.4 % in PV power output, which can reach 20 % during the dry season [46]. Furthermore, during the Harmattan season, a significant reduction of 29 % in PV performance has been documented due to dust accumulation [47]. Therefore, it is imperative to implement regular cleaning of the panels to ensure optimal photovoltaic performance, particularly in rural areas prone to significant dust buildup. However, the employment of manual cleaning methods that utilize detergents may lead to degradation of the panels, require considerable amounts of time, pose safety risks, and incur substantial costs.

A research endeavor by Tayel et al. [48] highlights the efficacy of PDMS/SiO_2 nanocoating in reducing dust accumulation on photovoltaic (PV) panels, enhancing solar energy production. This nanocoating outperformed commercial coatings and uncoated panels, resulting in a 31 % increase in efficiency after 40 days of outdoor exposure. Additionally, the effectiveness of super-hydrophilic coatings in minimizing dust deposition on solar PV surfaces during water spraying was explored. Findings show that these coatings significantly reduce dust and improve spectral transmittance, achieving 92 % greater self-cleaning efficiency than uncoated glass panels. Another study on a hydrophobic nanocoating reported a 13 % increase in power generation and a 50 % reduction in water consumption compared to uncoated panels [49].

Lukong et al. [50] studied titanium dioxide (TiO_2) thin films for self-cleaning photovoltaic (PV) applications, revealing that sol-gel-synthesized TiO_2 with a snowflake-like morphology of primarily anatase. It showed strong superhydrophilic properties and effective UV-visible light absorption, enhancing self-cleaning and photocatalytic activities in PV panels. Adak et al. developed a transparent, self-cleaning coating for PV modules via sol-gel processing, achieving a static contact angle of 150° and a hysteresis of approximately 2° [51]. This coating improved solar glass transmission from 91.8 % to 95.5 % and reduced reflectance from 8.7 % to 3.2 %, thanks to its antireflective properties. Another study highlighted a nitrogen-doped TiO_2/single-wall carbon nanotube nanocomposite for self-cleaning coatings on solar PV panels, achieving a 72.4 % degradation rate for Methylene Blue and a wettability of $94.3 \pm 2°$, ensuring sustained solar cell output despite dust accumulation [52]. Additionally, research presented a superhydrophobic and anti-reflective coating with a double-layer film structure, yielding increased adhesion, mechanical stability, and a 5 % boost in glass transmittance. This coating raised the maximum output power of PV modules by 5.7 % and restored power to 97 % during simulated dust and rainfall tests, compared to 83 % for uncoated modules [53].

4. CONCLUSIONS

The durable, multifunctional nanocomposite coatings developed in this work effectively enhance solar panel performance through a complementary interplay of self-cleaning, UV protection, and thermal management properties. FTIR analysis confirmed strong interfacial interactions among TiO_2, ZnO, and SiO_2 nanoparticles, which are critical for coating stability. The coating's properties work synergistically: high UV absorption (>0.87 a.u.) protects the polymer matrix, preserving the superhydrophobic surface (contact angle >140°) for self-cleaning; the self-cleaning property prevents dust accumulation and maintains light transmittance; and enhanced infrared emissivity (~84.7%) facilitates heat dissipation. Field testing over 8 weeks demonstrated that the coated panels achieved 59 % higher power output than uncoated panels and reduced surface temperatures by up to 8.6 %, with sustained stability. These results highlight the advantage of integrating multiple performance-enhancing features into a single, durable coating to improve solar panel efficiency and operational lifespan.

REFERENCES

1. **Talal, H., Akroot, A., Al Maamori, M.H., Saud, A.N., Arslan, K.** Enhancing Solar Panel Efficiency with a Multifunctional Nanocomposite Coating: Self-cleaning and Cooling Properties of ZnO, SiO_2, and Chlorophyll Integration *Journal of Coatings Technology and Research* 22 (3) 2025: pp. 1065 – 1077. https://doi.org/10.1007/s11998-024-01032-0
2. **Seroka, N.S., Taziwa, R., Khotseng, L.** Solar Energy Materials-Evolution and Niche Applications: A Literature Review *Materials* 15 (15) 2022: pp. 5338. https://doi.org/10.3390/ma15155338
3. **Alarifi, I.M.** Advanced Selection Materials in Solar Cell Efficiency and Their Properties-A Comprehensive Review *Materials Today: Proceedings* 81 2023: pp. 403 – 414. https://doi.org/10.1016/j.matpr.2021.03.427

4. **Machín, A., Márquez, F.** Advancements In Photovoltaic Cell Materials: Silicon, Organic, and Perovskite Solar Cells *Materials* 17 (5) 2024: pp. 1165. https://doi.org/10.3390/ma17051165
5. **Centeno PAM:** Self-Cleaned Solar Cells with Super-Hydrophobic Photonic Nano-Structures. Universidade NOVA de Lisboa (Portugal); 2018.
6. **Karthikeyan, B., Sakthivel, A., Kumar, P.S., Hussain, S.** Effect of Bi Doping on The Electrochemical Behaviour of Mg_2SiO_4 Nanoparticle for Energy Storage Applications *Surfaces and Interfaces* 51 2024: pp. 104609. https://doi.org/10.1016/j.surfin.2024.104609
7. **Ammed, S.P., Prasad, A.R., Ullattil, S.G.** Self-Cleaning Surfaces: Experimental Advances and Surface Model Controversies. Photocatalysis, edited by Suresh C. Pillai and Vignesh Kumaravel, Berlin, Boston: De Gruyter, 2021: pp. 135. https://doi.org/10.1515/9783110668483-005
8. **Regmi, G.** Unlocking Multifunctional Advantages with Nanocomposites Coatings for Solar Cells: A Comprehensive Review *Curr Org Chem* 27 (22) 2023: pp. 1946 – 1959. https://doi.org/10.2174/0113852728281107231212044214
9. **Alhodaib, A., Yahya, Z., Khan, O., Equbal, A., Equbal, M.S., Parvez, M., Kumar Yadav, A., Idrisi, M.J.** Sustainable Coatings for Green Solar Photovoltaic Cells: Performance and Environmental Impact of Recyclable Biomass Digestate Polymers *Scientific Reports* 14 (1) 2024: pp. 11221. https://doi.org/10.1038/s41598-024-62048-5
10. **Gaddam, S.K., Pothu, R., Boddula, R.** Advanced Polymer Encapsulates for Photovoltaic Devices − A Review *Journal of Materiomics* 7 (5) 2021: pp. 920 – 928. https://doi.org/10.1016/j.jmat.2021.04.004
11. **Sinha, A., Sulas-Kern, D.B., Owen-Bellini, M., Spinella, L., Uličná, S., Pelaez, S.A., Johnston, S., Schelhas, L.T.** Glass/Glass Photovoltaic Module Reliability and Degradation: A Review *Journal of Physics D: Applied Physic* 54 (41) 2021: pp. 413002. https://doi.org/10.1088/1361-6463/ac1462
12. **Shi, B., Xie, L., Ma, B., Zhou, Z., Xu, B., Qu, L.** Preparation and Properties of Highly Transparent Sio_2 Aerogels for Thermal Insulation *Gels* 8 (11) 2022: pp. 744. https://doi.org/10.3390/gels8110744
13. **Hameed, A.S.H., Karthikeyan, C., Sasikumar, S., Kumar, V.S., Kumaresan, S., Ravi, G.** Impact of Alkaline Metal Ions Mg 2+, Ca 2+, Sr 2+ And Ba 2+ on The Structural, Optical, Thermal and Antibacterial Properties of Zno Nanoparticles Prepared by The Co-Precipitation Method *Journal of Materials Chemistry B* 1 (43) 2013: pp. 5950 – 5962. https://doi.org/10.1039/C3TB21068E
14. **Majdi, H.S., Saud, A., Al-Mamoori, M.** A Novel Nanocomposite (SR/HA/-Nzno) Material for Medical Application *In: 4th International Conference on Nanotechnologies and Biomedical Engineering: Proceedings of ICNBME-2019* 2020: pp. 333 – 341.
15. **Nosheen, S., Galasso, F.S., Suib, S.L.** Role of Ti−O Bonds In Phase Transitions of Tio_2 *Langmuir* 25 (13) 2009: pp. 7623 – 7630. https://doi.org/10.1021/la9002719
16. **Liu, Z., Davis, R.J.** Investigation of The Structure of Microporous Ti-Si Mixed Oxides by X-Ray, UV Reflectance, FT-Raman, and FT-IR Spectroscopies *The Journal of Physical Chemistry* 98 (4) 1994: pp. 1253 – 1261. https://doi.org/10.1021/j100055a035
17. **Dahash, F., Aobaid, A., Koç, E., Saud, A., Al Maamori, M.** Preparation and Characterization of Rubber-Lead Nanocomposite Material As A Protective Shield Against Cobalt Gamma Radiation *Digest Journal of Nanomaterials & Biostructures (DJNB)* 20 (1) 2025: pp. 239 – 252. https://doi.org/10.15251/DJNB.2025.201.239
18. **Amores, A.P., Ravishankar, A.P., Anand, S.** Design and Modelling of Metal-Oxide Nanodisk Arrays for Structural Colors and UV-Blocking Functions In Solar Cell Glass Covers *Photonics* 9 (5) 2022: pp. 273. https://doi.org/10.3390/photonics9050273
19. **Dey, T.** UV-Reflecting Sintered Nano-Tio2 Thin Film on Glass for Anti-Bird Strike Application *Surface Engineering* 37 (6) 2021: pp. 688 – 694. https://doi.org/10.1080/02670844.2020.1796900
20. **Queant, C., Blanchet, P., Landry, V., Schorr, D.** Effect of Adding UV Absorbers Embedded In Carbonate Calcium Templates Covered with Light Responsive Polymer Into A Clear Wood Coating Coatings 8 (8) 2018: pp. 265. https://doi.org/10.3390/coatings8080265
21. **Wang, J., Ma, L., Ding, X., Xu, H., Wang, Y., Zhao, M., Ren, C., Zhang, D.** Tea Polyphenol Radical Scavenger Loaded UV Absorber for Corrosion Resistant and Weathering Resistant Epoxy Coating Fabrication *Progress in Organic Coatings* 180 2023: pp. 107553. https://doi.org/10.1016/j.porgcoat.2023.107553
22. **Dong, W., Zhou, L., Guo, Y., Tang, Y., Pan, R., Liu, M., He, D.** Modification of Styrene-Acrylic Emulsion by Organic UV Absorber In Synergy With Fluorine and Silicon Monomers for Weatherable Coatings *Journal of Coatings Technology and Research* 19 (2) 2022: pp. 607 – 616. https://doi.org/10.1007/s11998-021-00550-5
23. **Nikafshar, S., Nejad, M.** Evaluating Efficacy of Different UV-Stabilizers/Absorbers In Reducing UV-Degradation of Lignin *Holz* 76 (3) 2022: pp. 235 – 244. https://doi.org/10.1515/hf-2021-0147
24. **Xi, L., Lv, Y., Feng, J., Huang, Y., Huang, Y., Yang, Q., Li, G., Kong, M.** Synthesis of UV-Resistant and Colorless Polyimide Films for Optoelectrical Applications *NPJ Materials Degradation* 8 (1) 2024: pp. 6. https://doi.org/10.1038/s41529-023-00422-w
25. **Yang, J., Wang, J., Strømme, M., Welch, K.** Enhanced UV Protection and Water Adsorption Properties of Transparent Poly (Methyl Methacrylate) Films Through Incorporation of Amorphous Magnesium Carbonate Nanoparticles *Journal of Polymer Research* 28 (8) 2021: pp. 281. https://doi.org/10.1007/s10965-021-02630-x
26. **Caseri, W.** Nanocomposites of Polymers and Inorganic Particles: Preparation, Structure and Properties *Materials Science and Technology* 22 (7) 2006: pp. 807 – 817. https://doi.org/10.1179/174328406X101256
27. **Caseri, W.** Inorganic Nanoparticles as Optically Effective Additives for Polymers *Chemical Engineering Communications* 196 (5) 2008: pp. 549 – 572. https://doi.org/10.1080/00986440802483954
28. **Caseri, W.** Nanocomposites of Polymers and Metals or Semiconductors: Historical Background and Optical Properties *Macromolecular Rapid Communications* 21 (11) 2000: pp. 705 – 722. https://doi.org/10.1002/1521-3927(20000701)21:11%3C705::AID-MARC705%3E3.0.CO;2-3

29. **Kubacka, A., Fernandez-Garcia, M., Colon, G.** Advanced Nanoarchitectures for Solar Photocatalytic Applications *Chemical Reviews* 112 (3) 2012: pp. 1555 – 1614. https://doi.org/10.1021/cr100454n
30. **Dutta, K., De, S.K.** Electrical Conductivity and Dielectric Properties of SiO_2 Nanoparticles Dispersed In Conducting Polymer Matrix *Journal of Nanoparticle Research* 9 (4) 2007: pp. 631 – 638. https://doi.org/doi.org/10.1007/s11051-006-9184-4
31. **Matsuyama, K., Mishima, K., Kato, T., Irie, K., Mishima, K.** Transparent Polymeric Hybrid Film of Zno Nanoparticle Quantum Dots And PMMA with High Luminescence and Tunable Emission Color *Journal of Colloid and Interface Science* 367 (1) 2012: pp. 171 – 177. https://doi.org/10.1016/j.jcis.2011.10.003
32. **Barshilia, H.C., John, S., Mahajan, V.** Nanometric Multi-Scale Rough, Transparent and Anti-Reflective Zno Superhydrophobic Coatings on High Temperature Solar Absorber Surfaces *Solar Energy Materials and Solar Cells* 107 2012: pp. 219 – 224. https://doi.org/10.1016/j.solmat.2012.06.031
33. **Agustín-Sáenz, C., Machado, M., Zubillaga, O., Tercjak, A.** Hydrophobic and Spectrally Broadband Antireflective Methyl-Silylated Silica Coatings with High Performance Stability for Concentrated Solar Applications *Solar Energy Materials and Solar Cells* 200 2019: pp. 109962. https://doi.org/10.1016/j.solmat.2019.109962
34. **Nagel, H., Aberle, A.G., Hezel, R.** Optimised Antireflection Coatings for Planar Silicon Solar Cells Using Remote PECVD Silicon Nitride and Porous Silicon Dioxide *Progress in Photovoltaics: Research and Applications* 7 (4) 1999: pp. 245 – 260. https://doi.org/10.1002/(SICI)1099-159X(199907/08)7:4%3C245::AID-PIP255%3E3.0.CO;2-3
35. **Luo, Q., Deng, X., Zhang, C., Yu, M., Zhou, X., Wang, Z., Chen, X., Huang, S.** Enhancing Photovoltaic Performance of Perovskite Solar Cells with Silica Nanosphere Antireflection Coatings *ACS Appl Mater Interfaces* 169 2018: pp. 128 – 135. https://doi.org/10.1021/acsami.7b10101
36. **Xia, R., Zhang, B., Dong, K., Yan, Y., Guan, Z.** HD-Sio_2/Sio_2 Sol@ PDMS Superhydrophobic Coating with Good Durability and Anti-Corrosion for Protection of Al Sheets *Materials* 16 (9) 2023: pp. 3532. https://doi.org/10.3390/ma16093532
37. **Ogihara, H., Xie, J., Okagaki, J., Saji, T.** Simple Method for Preparing Superhydrophobic Paper: Spray-Deposited Hydrophobic Silica Nanoparticle Coatings Exhibit High Water-Repellency and Transparency *Langmuir* 28 (10) 2012: pp. 4605 – 4608. https://doi.org/10.1021/la204492q
38. **de Jesus, M., Timò, G., Agustín-Sáenz, C., Braceras, I., Cornelli, M., de Mello Ferreira, A.** Anti-Soiling Coatings For Solar Cell Cover Glass: Climate and Surface Properties Influence *Solar Energy Materials and Solar Cells* 185 2018: pp. 517 – 523. https://doi.org/10.1016/j.solmat.2018.05.036
39. **Jang, G.G., Smith, D.B., Polizos, G., Collins, L., Keum, J.K., Lee, D.F.** Transparent Superhydrophilic and Superhydrophobic Nanoparticle Textured Coatings: Comparative Study of Anti-Soiling Performance *Nanoscale Advances* 1 (3) 2019: pp. 1249 – 1260. https://doi.org/10.1039/C8NA00349A
40. **Chen, G., Wang, Y., Qiu, J., Cao, J., Zou, Y., Wang, S., Ouyang, J., Jis, D., Zhou, Y.** A Visibly Transparent Radiative Cooling Film With Self-Cleaning Function Produced By Solution Processing *Journal of Materials Science & Technology* 90 2021: pp. 76 – 84. https://doi.org/10.1016/j.jmst.2021.01.092
41. **Chikate, B.V., Sadawarte, Y., Sewagram, B.** The Factors Affecting The Performance of Solar Cell *In: International Journal of Computer Applications* 2015: pp. 0975 – 8887.
42. **Chanchangi, Y.N., Ghosh, A., Baig, H., Sundaram, S., Mallick, T.K.** Soiling on PV Performance Influenced by Weather Parameters In Northern Nigeria *Renewable Energy* 180 2021: pp. 874 – 892. https://doi.org/10.1016/j.renene.2021.08.090
43. **Dida, M., Boughali, S., Bechki, D., Bouguettaia, H.** Output Power Loss of Crystalline Silicon Photovoltaic Modules Due to Dust Accumulation In Saharan Environment *Renewable and Sustainable Energy Reviews* 124 2020: pp. 109787. https://doi.org/10.1016/j.rser.2020.109787
44. **Adinoyi, M.J., Said, S.A.** Effect of Dust Accumulation on The Power Outputs of Solar Photovoltaic Modules *Renewable Energy* 60 2013: pp. 633 – 636. https://doi.org/10.1016/j.renene.2013.06.014
45. **Kimber, A., Mitchell, L., Nogradi, S., Wenger, H.** The Effect of Soiling on Large Grid-Connected Photovoltaic Systems In California and The Southwest Region of The United States *In: 2006 IEEE 4th World Conference on Photovoltaic Energy Conference IEEE* 2006: pp. 2391 – 2395.
46. **Zorrilla-Casanova, J., Piliougine, M., Carretero, J., Bernaola-Galván, P., Carpena, P., Mora-López, L., Sidrach-de-Cardona, M.** Losses Produced By Soiling In The Incoming Radiation to Photovoltaic Modules *Progress in Photovoltaics: Research and Applications* 21 (4) 2013: pp. 790 – 796. https://doi.org/10.1002/pip.1258
47. **Bernard, O.** The Effect of Settling Harmattan Dust on Photovoltaic Modules In Walewale, Northern Ghana. Kwame Nkrumah University of Science and Technology, 2016.
48. **Tayel, S.A., Abu El-Maaty, A.E., Mostafa, E.M., Elsaadawi, Y.F.** Enhance The Performance of Photovoltaic Solar Panels by A Self-Cleaning and Hydrophobic Nanocoating *Scientific Reports* 12 (1) 2022: pp. 21236. https://doi.org/10.1038/s41598-022-25667-4
49. **Aljdaeh, E., Kamwa, I., Hammad, W., Abuashour, M.I., Sweidan, T., Khalid, H.M., Muyeen, S.** Performance Enhancement of Self-Cleaning Hydrophobic Nanocoated Photovoltaic Panels In A Dusty Environment *Energies* 14 (20) 2021: pp. 6800. https://doi.org/10.3390/en14206800
50. **Lukong, V., Mouchou, R., Enebe, G., Ukoba, K., Jen, T.** Deposition And Characterization of Self-Cleaning Tio_2 Thin Films for Photovoltaic Application *Materials Today: Proceedings* 62 2022: pp. S63 – S72. https://doi.org/10.1016/j.matpr.2022.02.089
51. **Adak, D., Bhattacharyya, R., Saha, H., Maiti, P.S.** Sol–Gel Processed Silica Based Highly Transparent Self-Cleaning Coatings for Solar Glass Covers *Materials Today: Proceedings* 33 2020: pp. 2429 – 2433. https://doi.org/10.1016/j.matpr.2020.01.331

52. **Appasamy, J.S., Kurnia, J.C., Assadi, M.K.** Synthesis and Evaluation of Nitrogen-Doped Titanium Dioxide/Single Walled Carbon Nanotube-Based Hydrophilic Self-Cleaning Coating Layer for Solar Photovoltaic Panel Surface *Solar Energy* 196 2020: pp. 80 – 91. https://doi.org/10.1016/j.solener.2019.12.022

53. **Wang, P., Yan, X., Zeng, J., Luo, C., Wang, C.** Anti-Reflective Superhydrophobic Coatings with Excellent Durable and Self-Cleaning Properties for Solar Cells *Applied Surface Science* 602 2022: pp. 154408. https://doi.org/10.1016/j.apsusc.2022.154408